Effect of Steaming Treatment in the Structure and Reactivity of FCC Catalysts

G. M. Tonetto and M. L. Ferreira
Chemical Engineering Dept. PLAPIQUI - (UNS-CONICET) - Camino La Carrindanga Km 7 - CC 717 - (8000) Bahía Blanca – Argentina

J. A. Atias and H. I. de Lasa
Chemical Reactor Engineering Centre, Faculty of Engineering Science, University of Western Ontario, London, Ontario, Canada N6A 5B9

DOI 10.1002/aic.10629
Published online November 11, 2005 in Wiley InterScience (www.interscience.wiley.com).

The shape selectivity properties of USY zeolite crystallites is discussed, and is based on catalyst characterization, molecular simulation, catalytic experiments of model compounds and kinetic modeling. Typical FCC catalysts are prepared with different HY crystallite sizes (0.4 and 0.9 μm), and are structurally and chemically characterized with nitrogen and argon adsorption/desorption isotherms, temperature-programmed desorption of ammonia and infrared spectroscopy. Catalyst characterization is carried out before and after the hydrothermal treatment (steaming) of the catalyst. Pore-size distribution analysis demonstrates that the effect of the steaming treatment in the Y zeolite results in window enlargement. The influences of structural changes of steam treatment on reactivity is evaluated with the catalytic conversion of 1,2,4-trimethylbenzene in a novel fluidized CREC riser simulator. It is proven that steaming enlarges zeolite windows and influence the 1,2,4-TMB product distribution. A slight modification of the window diameter is proven to significantly affect the adsorbent-adsorbate interactions. Focus is particularly given to the catalyst selectivity toward the tetramethylbenzene isomers, and the "transition-state shape selectivity" is proven to be controlling the product distribution and is consistent with molecular mechanics calculations. © 2005 American Institute of Chemical Engineers *AIChE J,* 52: 754–768, 2006
Keywords: zeolite; steaming treatment; kinetic modeling; molecular simulation; shape selectivity

Introduction

With over 1 million tons/day of oil processed in the world, catalytic cracking is the first and most widely used refinery process in the conversion of heavy oils to valuable gasoline and lighter products.[1,2] Cracking processes were first carried out without catalysts, but in the past six decades improved series of cracking catalysts has been continuously applied, all of which are solid acids. In the past three decades a most important advance in cracking technology has been the introduction and the development of zeolite catalysts.

Central to a successful catalytic process is the development of an effective catalyst, which is often a complex system in terms of both composition and functionality. The ability to control the microstructure and the chemistry of catalysts allows for the systematic manipulation of its activity, selectivity, and stability.[3]

Fluid catalytic cracking (FCC) catalysts are in the form of

Correspondence concerning this article should be addressed to H. de Lasa at hdelasa@eng.uwo.ca.

fine powders with an average particle size in the range of 75–50 μm. A modern FCC catalyst has four major components: zeolite, matrix, binder, and filler.[4,5] Zeolites employed in the manufacture of the FCC catalysts are synthetic versions of naturally occurring zeolites called faujasites. Some of the earlier FCC zeolite catalysts contained X zeolite; however, virtually all of today's catalysts contain Y zeolite or variation thereof. Particular characteristics of zeolites are their crystalline structure and acidity that are responsible for their capability to catalyze chemical reactions. In Y zeolites, twelve member oxygen rings delimit the 0.74 nm opening windows connecting 1.2 nm-dia.-supercages and conform the three-dimensional (3-D) pore network.[6]

Y-type zeolites can undergo hydrothermal treatment producing the so-called ultrastable Y (USY) zeolites where framework dealumination takes place.[7] Associated with this hydrothermal treatment are predominantly three structural changes in the zeolite that are well documented in the literature:

- Partial destruction of zeolite framework: Electron microscopy studies of USY zeolites show the presence of a substantial number of mesopores that increases the densities of fissures and crevices.[8,9,10]
- Removal of framework aluminum ions from the crystalline zeolite: These ions removed from the crystalline structure remain in the crystallite as non- or extra-framework aluminum (EFAL) species.[11,12,13,14]
- Appearance of new Lewis acid sites and hydroxyl groups: When aluminum is extracted from the zeolite framework, two distinct types of acidic sites (Brönsted and Lewis) are located both in the internal pore structure and on the outside surface of the crystallites.[15] These changes can be monitored spectroscopically[16] and calorimetrically.[17,18,19]

The overall consequence of hydrothermal treatment is that the USY zeolite becomes much more active for cracking, sometimes by nearly two orders of magnitude compared to nonhydrothermally treated catalysts (Y zeolite).[20]

An explanation for the enhanced catalyst activity assumes that the cracking reaction in Y and USY zeolites is limited by diffusion in the micropores.[21,22,23] Mesopores, crevices, and fissures formed in the zeolite crystallite during the dealumination process increase the accessibility of the internal acid sites in the crystalline pore network.[24] These structural changes in the crystallite are also expected to modify the pore diameter distribution with an increase in the average pore size.

In zeolites, diffusing molecules with molecular size comparable to the pore dimensions of Y and USY zeolites may not pass each other. Therefore, diffusion takes place in the "configurationa" regime, with diffusion becoming unidirectional and greatly reduced as the result of molecules constrained transport.[25]

Kung et al.[26] analyzed USY zeolites during the cracking of hydrocarbons and observed that depending on the reaction conditions (reactant and product partial pressures, temperature), the predominant cracking reaction mechanism might differ. It was also speculated that changes in the predominant mechanism might also be a consequence of the proportionally small increase in external specific surface area caused by the steaming-induced structural destruction of the zeolite particles. These relatively small changes in the zeolite structure can lead to large overall effects on the cracking rates and cracking mechanism.

In order to clarify the role of intracrystalline diffusion in USY zeolites, catalytic experiments using 1,2,4-trymethylbenzene (1,2,4-TMB) and typical FCC catalysts of different crystallite sizes are performed in a CREC Riser Simulator. This bench-scale reactor overcomes the limitations of other laboratory scale reactors by closely simulating the reaction conditions of industrial FCC units in terms of: temperature, reaction time, partial pressure of hydrocarbons, and catalyst/oil ratio. All this provides realistic results for studying chemical changes in the context of steam-modified zeolites.

Recent reports from Smit and Krishna[27] demonstrated that molecular simulation techniques provide estimates of data and valuable insights in the design of processes using zeolite adsorbents or catalysts. In this study, the main objective was to study the interaction of probes molecules such as 1,2,4 TMB with the structure of the USY zeolite, having available experimental data on the activity and selectivity of 1,2,4 TMB catalytic transformation. For many catalytic systems involving zeolites the molecules diffuse very slowly, and as a consequence the total simulation time needed to compute a diffusion coefficient can become prohibitely large. To overcome this limitation a different approach, that deals with steric energies and provides a sense of the accessibility to the zeolite window, is considered in this study. In this manner, new insights are provided into the process of configurational diffusion of bulky molecules through the USY zeolite pore network.

From all the early, this study addresses a relevant issue on the design of FCC catalysts which is the effect of hydrothermal treatment in the structure and reactivity of FCC catalysts. Activity and distribution of products during the catalytic cracking of the model compound is explained in terms of shape-selectivity concepts, and validated by the catalyst characterization and molecular simulation. Experimentation with FCC catalysts manufactured under similar conditions, but differing in crystallite size, is advantageous to identify the effect of diffusion on the activity and the selectivity of the catalyst.

Experimental Section

Catalysts preparation

Two crystallite sizes (0.4 and 0.9 μm) were employed to manufacture typical commercial FCC catalysts. The parent Y zeolites were spray-dried using kaolin as the filler and silica sol as the binder. The resulting catalyst pellets (30 wt. % Y zeolite, 50 wt. % kaolin and 20 wt. % silica sol) displayed an average particle size of 60 μm. The catalysts were ion exchanged with NH_4NO_3 and then calcined at 600°C for 2 h to remove all volatile material. CAT-SC-BS and CAT-LC-BS are acronyms used to refer to catalyst samples before the steaming treatment, indicating catalysts containing small and large crystallites, respectively. To increase the thermal and hydrothermal stability, the catalysts were treated with 100% steam for 5 h at 760°C. In this study, CAT-SC and CAT-LC are acronyms used to refer to catalyst samples after the steaming treatment, indicating catalysts containing small and large crystallites. Table 1 reports the main properties defining the characterization of the FCC catalysts after the hydrothermal treatment. Additional details about catalyst preparation can be found in Tonetto et al.[28]

Table 1. Properties of the Small (CAT-SC) and the Large (CAT-LC) Crystallite Catalysts after the Steaming Treatment

	CAT-SC	CAT-LC
Zeolite content [wt%]	31	29
Unit cell size [nm]	2.428	2.427
USY crystallite size [μm]	0.4	0.9
NH_3 desorbed @ 140°C [mmol NH_3/g HY]	0.21	0.18
Brönsted/Lewis Sites ratio @ 100°C	0.9	1

Catalysts characterization

Temperature-Programmed Desorption – TPD. Temperature-programmed desorption of ammonia is a useful technique of characterization. Because of its weak basicity and small molecular dimensions, ammonia is a suitable probe for all hydroxyl groups accessible through pores $\geq$ 0.4 nm.[24]

The apparatus used for the temperature programmed desorption (TPD) test was the Micromeritics AutoChem II analyzer. A sample (0.1–0.3 g) contained in a quartz container was degassed for 2 h at 500°C and saturated with an NH_3/He gas mixture (4.45% ammonia, 95.55% helium). Ammonia adsorption was carried out for 1 h at 140°C to assess the acidity of active sites. To remove physically adsorbed ammonia, the ammonia flow was switched off and replaced by an inert purge gas (He) at a rate of 50 mL/min for 1 h at 140°C. Then, the temperature was raised at a rate of 15°C/min and NH_3-TPD chromatograms were collected. The total flow used was 50 mL/min (STP).

Fourier transform infrared spectroscopy - FTIR

Since NH_3-TPD cannot distinguish between Brönsted and Lewis-type sites, an alternative experimental tool was used to further characterize the FCC catalyst acidity. To overcome the limitations of NH_3-TPD experiments, fourier transform infrared spectroscopy (FTIR) analysis of preadsorbed pyridine was implemented. This technique establishes the relative abundance of Brönsted and Lewis acid sites in the various samples.

The lone-pair electrons of nitrogen in pyridine are involved in different types of interactions with the surface acid sites. Their IR absorption bands can identify these interactions.[30] Pyridine coordinated with a Lewis site yields a peak at 1,450 cm^{-1} and protonated pyridine on a Brönsted center gives a peak at 1,540 cm^{-1}. The 1,600 cm^{-1} band is generally assigned to hydrogen-bonded pyridine. On the basis of previous studies presented by Rosenthal et al.[31] and Emeis,[32] this method was used to determine a Brönsted/Lewis (B/L) ratio.

Samples were dried *in situ* by heating under N_2 flow at 550°C and then cooled to 100°C. The samples were maintained at this temperature and saturated with pyridine using a N_2-pyridine stream. Adsorption of pyridine was performed for a 60 min period. Then, the zeolite was flushed with N_2, at the same temperature for 90 min, and this to remove weakly adsorbed pyridine species.

After this pretreatment of the samples, diffuse reflectance infrared spectroscopy (DRIFTS) measurements were recorded using a Bruker IFS55 FTIR spectrometer operating at 4 cm^{-1} resolution and 100 scans. FTIR spectra were collected at room temperature.

Nitrogen and Argon Isotherms

The microstructure of FCC catalysts (specific surface area, pore size and pore-size distribution) was studied by analysis of nitrogen and argon adsorption isotherms at 77 K.

The apparatus used for nitrogen and argon adsorption measurements was the Micromeritics ASAP 2010 automatic adsorption analyzer. Samples (0.1 to 0.3 g) were consecutively degassed for 1h at 100°C and for 10 h at 300°C. The samples were then contacted with different concentrations of either nitrogen or argon at 77 K. Adsorption isotherms were measured in the relative pressure 10^{-6} to 1 range, based on the saturation vapor pressure of the adsorbate.

Micropore-size distributions were obtained from the Horvath-Kawazoe equation and density functional theory (DFT).[33] The DFT formalism has in recent years received considerable attention as a way to describe the adsorption process at a gas/solid interface of pores with slit-like or cylindrical geometry.[34] The ability of the DFT to model physical adsorption provides a suitable method to extract the specific surface area and the pore size distribution from experimental adsorption isotherms. Porosity distribution by DFT was obtained using nitrogen isotherm data collected at 77 K, and a model for cylindrical pores.

Catalytic experiments

Catalytic experiments of 1,2,4-TMB (Aldrich, +98% purity) were performed in a novel CREC riser simulator. This unit is an experimental reactor, which combines a batch of catalyst and a batch of fluid operating isothermally, and at constant volume of reaction mixture. Experiments were carried out at various temperatures (350, 400, 450, 500, and 550°C) and residence times (3, 5, and 7 s), with a catalyst-to-hydrocarbon ratio of 5 and reactant partial pressure between 100 – 150 kPa. An average of ten experimental runs was carried out for every different pair of temperature and residence time, giving a total of about 150 experiments for each catalyst. This significant number of catalytic runs ensured consistency in results and provided low data dispersion, with experimental mass fractions of products in the 5–3% error range.

The CREC riser simulator invented by de Lasa[35] is a well-mixed and bench-scale device that enables the reacting chemical species to come into contact with fluidized catalyst throughout a predetermined time span. The 52 cm^3 CREC riser simulator reactor and its components is presented in Figure 1. Isothermal operation conditions are reached given the special design of this unit plus the relatively small amount of reacting species (0.162 g) and catalysts (0.81 g). Additional description of the operation and assembly of the CREC riser simulator can be found in Atias et al.[36]

An average of ten experimental runs was carried out for every different pair of temperature and residence time, giving a total of about 150 experiments for each catalyst. This significant number of catalytic runs ensured consistency in results and provided low data dispersion, with experimental mass fractions of products in the 5–3% error range.

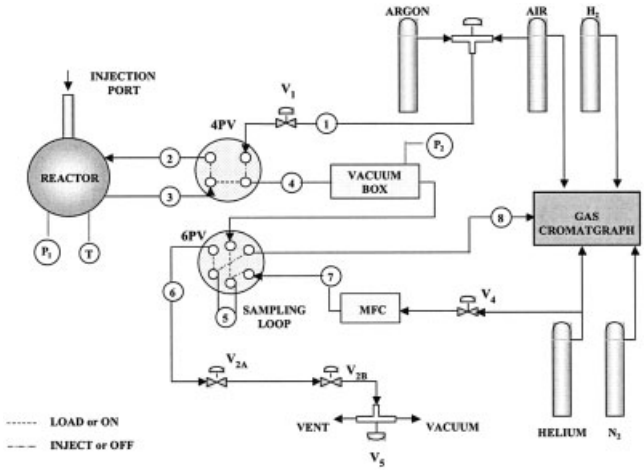

Figure 1. CREC riser simulator.

Experimental set-up and accessories.

Molecular Modeling and Analysis

Molecular modeling of USY zeolite

As introduced in previous sections, Y zeolites consist of tetrahedrons (four oxygen anions surrounding a silicon or aluminum ion) linked to form cube-octahedrons (sodalite cage units) as shown in Figure 2A. A sodalite or truncated octahedron contains 24 silica and alumina tetrahedrons. Each sodalite unit in the structure is connected to four other sodalite units by six bridge oxygen ions connecting the hexagonal faces of two units. Surrounded by ten sodalite units, the structure results in a supercage (sorption cavity) which is sufficiently large for an inscribed sphere with a diameter of ~1.2 nm. The opening into this large cavity is bounded by sodalite units, resulting in a 12-membered oxygen ring with a theoretical 0.74 nm free dia. Each cavity is connected to four other cavities, which are themselves connected to 3-D cavities to form a highly porous framework structure. It is within this pore structure that the locus of catalytic activity resides for many reactions.

The molecular model was based in the window of the USY zeolite (as shown in Figure 2), which was built from 6 sodalite cages and the corresponding hexagonal prisms.[37] The SiO_2/$Al2O_3$ ratio used in the model corresponded to the experimental value obtained in the characterization of USY zeolites, which was equal to 5.6. It was assumed that the distribution of EFAL was in the crystalline portion of USY as experimentally found by by Gola et al.[38] in studies performed on steamed USY zeolite samples. It was found experimentally in this study that the hydrotreatment relaxes the crystalline structure of the parent zeolite (Y zeolite) by expanding the window diameter from 0.74 (Figure 2A) to 0.81 nm (Figure 2B).

Two USY zeolite structures were considered in this molecular modeling study. Both models included hydrogen, aluminum, silicon and oxygen atoms. Si-O bond length was assumed to be 0.1675 nm whereas the length of the Al-O bond located in the plane defined by the 12-oxygen-membered window was between 0.1794 nm and 0.1840 nm. The length of Al-O bond located outside of the window's plane was assumed to be equal to 0.2024 nm (see Figure 2).

Selected probe molecules were considered and their interaction with the two USY zeolite structures was studied in order to explain the potential diffusion limitations and shape-selectivity effect of zeolite catalysts.

Molecular modeling and analysis

The molecular modeling and analysis of probe molecules interacting with the USY zeolite structure was performed using CS Chem3D (version 5.0), which is a software developed by Cambridge Soft. Chem 3D is used to carry out both molecular mechanics (MM2) and molecular orbital calculations (MOPAC-PM3). Therefore, Chem3D provided insight into the conformational properties of the model compound molecules and their interaction with the window of the USY zeolite crystalline structure.

Molecular Mechanics - MM2

A Molecular Mechanic program (MM2) was implemented to optimize geometry and determine thermodynamic values. The Chem 3D version of the MM2 method was used to evaluate the steric energy of various probe molecules and the window of USY zeolite (six-membered sodalite cages) in order to find potential energy minima.

Molecular Orbital Package - MOPAC-PM3

Molecular Orbital Package (MOPAC) is a general-purpose semiempirical molecular orbital package included in Chem 3D and developed by Dudek and Ponder.[39] This package contains the Parametrized Model revision 3 (PM3) Hamiltonians, which were employed to analyze the changes in enthalpy upon 1,2,4-TMB adsorption and reaction. While the MM2 method described earlier is useful for ground state calculations, it is not parameterized for excited state studies.

Parametrized model revision 3 (PM3) is a reparametrization of Austin Model 1 (AM1). Hypervalent compounds are predicted with significant improved accuracy and overall errors in formation enthalpies are reduced by about 40%.

Results and Discussion

Catalysts characterization

Once the catalysts were prepared with small (0.4 μm) and large (0.9 μm) USY crystallites, various samples of catalysts before and after steaming were characterized using surface science techniques explained in previous sections. Sodium content was found negligible in all samples after ion exchange.

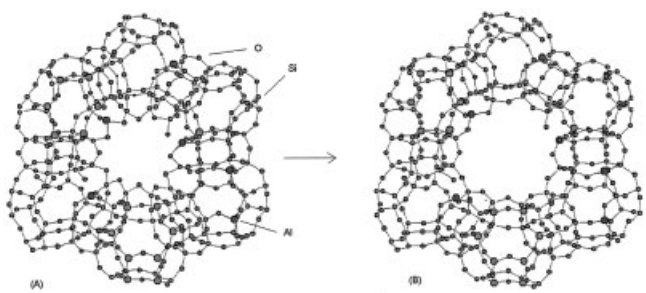

Figure 2. Molecular simulation of a nonrelaxed (A) and "relaxed" (B) USY zeolite window as predicted with MM2 method.

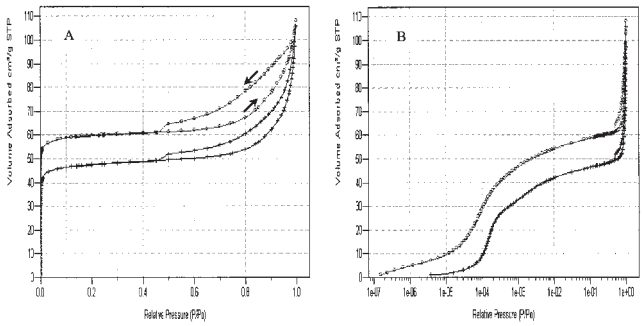

Figure 3. Adsorption-desorption isotherms of nitrogen on small crystallite catalysts before steaming ((○) CAT-SC-BS) and after steaming ((+) CAT-SC).

(A) Volume adsorbed as a function of relative partial pressure, and (B) Volume adsorbed vs. the logarithm of relative partial pressure.

Table 1 shows the main properties for the USY zeolite catalysts after steaming. For both crystallite size catalysts, the initial unit cell size (UCS) of 2.45 nm was reduced to 2.43 nm after the steaming treatment. Dealumination of the crystalline structure of the USY zeolite occurs when catalysts undergo steaming treatment; therefore, reduction of UCS is expected because of a higher abundance of Si-O bonds, which are shorter than Al-O bonds. Table 1 also shows that both catalysts prepared under the same conditions display similar properties in terms of total acidity (NH_3-TPD) and Brönsted/Lewis Sites ratio (Pyridine IR), as explained further in following sections.

Temperature-programmed desorption of ammonia - NH_3-TPD

Separate experiments performed with pellets of matrix only (no USY crystallite supported) showed that the NH_3 adsorption on the silica matrix was insignificant, which indicated the inert nature of the matrix.

The amount of desorbed ammonia is summarized in Table 1 for the catalyst samples after steaming. It can be observed that the amount of ammonia desorbed from both FCC catalysts were similar (average ~0.2 mmol/g). Ammonia TPD results for catalysts without steaming treatment were also comparable for both samples: ~1.1 mmol/g. Consequently, concerning the acidity of the catalyst before and after steaming, a decrease of about 85% of total adsorbed ammonia was observed for the two catalysts following steaming.

Fourier Transform Infrared Spectroscopy - Pyridine FTIR

Table 1 reports the Brönsted/Lewis ratio showing that this value was similar for both catalysts with no observable pyridine adsorption on the matrix. It is interesting to indicate that B/L ratio decreased 10% after steaming treatment. This change can be attributed to the formation of extra-framework aluminum in the crystalline structure after the steaming process. Brönsted sites are reduced and Lewis sites are created with the dealumination of the crystalline structure of the USY zeolite.

Nitrogen and Argon Isotherm

Figures 3 and 4 report the nitrogen adsorption-desorption isotherms of CAT-SC and CAT-LC, respectively, before and after steaming. Note that in order to have a detailed observation of the micropore region, Figures 3B and 4B are presented as semilog plots.

The shape of the adsorption isotherms of FCC catalysts is Type I in the Brunauer, Deming, Deming and Teller classification, which is typical of microporous solids. These isotherms indicate that the main difference between the samples is the adsorption ability at low relative pressures. It appears that the steamed CAT-SC catalyst has a lower total pore volume than the same catalyst sample before the steaming treatment (CAT-SC-BS). This observation was not so noticeable for the case of large crystallite catalysts. On the other hand, the parallelism of the isotherms after micropore filling indicates little change in the mesopores structure. The small parallel hysteresis loops observed in Figures 3 and 4 are typical of solids, such as FCC catalysts, which contain slit-shaped mesopores resulting from the presence of kaolin platelets. Similar observations can be obtained comparing the argon adsorption isotherms. Moreover, it can be concluded that in the FCC catalysts of this study, zeolite crystallites are the major contributor to the microporosity and that the matrix is the major supplier of mesoporosity.

The specific surface area (SSA), pore volume and median pore diameter computed from the nitrogen and argon isotherms for samples of catalysts before and after steaming are shown in Table 2. The specific surface area decreased as a consequence of the severe steaming pretreatment for both small and large crystallite catalysts, being this observation more notorious in CAT-SC than in CAT-LC. Table 2 shows external specific surface areas of 25 and 20 m^2/g for CAT-SC and CAT-LC, respectively, reflecting the effect of the difference in crystallite sizes. Since both small and large crystallite catalysts were manufactured with similar amounts (mass basis) of zeolite crystallites; the CAT-SC was expected to have a larger external specific surface area than the one for the CAT-LC.

Table 2 shows that the micropore volume decreased in the small crystallite catalysts as a consequence of the severe steaming pretreatment. However, this reduction in micropore volume was not observed in the case of the large crystallite catalysts.

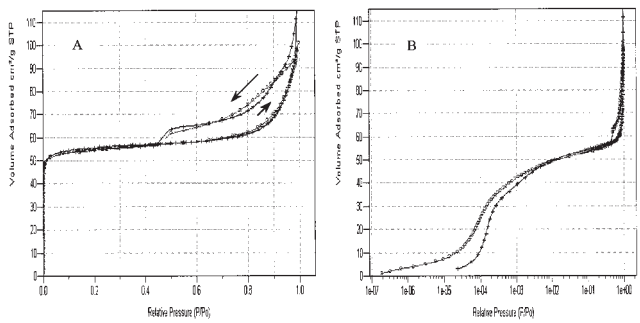

Figure 4. Adsorption-desorption isotherms of nitrogen on large crystallite catalysts before steaming ((○) CAT-LC-BS) and after steaming ((+) CAT-LC).

(A) Volume adsorbed as a function of relative partial pressure, and (B) Volume adsorbed vs. the logarithm of relative partial pressure.

Table 2. Specific Surface Area (SSA), Specific Pore Volume (SPV), and Median Pore Diameter [Å] of the Small (CAT-SC) and the Large (CAT-LC) Crystallite Catalysts before and after Steaming Treatment

	Before Steaming		After Steaming	
	CAT-SC-BS	CAT-LC-BS	CAT-SC	CAT-LC
SSA − BET[A] (m^2/g)	213	198	169	197
Micropore SSA − t-Plot[B] (m^2/g)	187	178	144	177
External SSA − t-Plot (m^2/g)	25	20	25	20
Micro SPV − t-plot (cm^3/g)	0.082	0.072	0.062	0.072
Total SPV[C] (cm^3/g)	0.150	0.139	0.133	0.143
Mean pore diameter − N_2[D] (nm)	0.75 1.05	0.76 1.04	1.12	1.11
Mean pore diameter − Ar[D] (nm)	1.25	1.23	1.27	1.28

A. Calculated using the BET equation[59] in the range $0.05 < P/P_0 < 0.33$.
B. Calculated using the t-plot method[60]: Thickness Curve Type Harkins and Jura: $t\text{-}plot = [13.99/(0.034 - lg(P/P_0)]^{0.5}$.
C. Measured at $P/P_0 \sim 0.98$.
D. Cylindrical-pore geometry (Saito and Foley) and Cheng and Yang correction.

Comparing values for the small and large crystallite catalysts, it seems that the steaming treatment is more effective on the small crystallite catalysts.

Table 3 displays the values of physical properties for adsorbates (nitrogen and argon) and adsorbent (USY zeolite) used in the pore-size distribution (PSD) calculations based on the Horvath-Kawazoe model.[40] The median pore diameters obtained from nitrogen and argon isotherms are included in Table 2.

Figures 5A shows the micropore-size distribution obtained from nitrogen adsorption isotherms of small crystallite catalysts before (CAT-SC-BS; void circle) and after (CAT-SC; crosses) steaming treatment. Figure 5A shows that the CAT-SC-BS exhibited two peaks, one at ~0.75 nm and the other at ~1.05 nm. After dealumination or steaming treatment, the first peak disappears while the second peak shifts to ~1.12 nm. Similar observations can be stated from Figure 5B for the case of large crystallite catalysts.

As noted earlier, the DFT and the Horvath-Kawazoe models applied to the N_2 isotherms yield two pore sizes. This is consistent with the findings of other researchers,[41] who ascribed this result to the level of polarization of the probe molecule and the degree of dealumination of the zeolitic structure.

Despite the experimental results and in view of the spatial structural ordering of the studied zeolites, a single pore size is

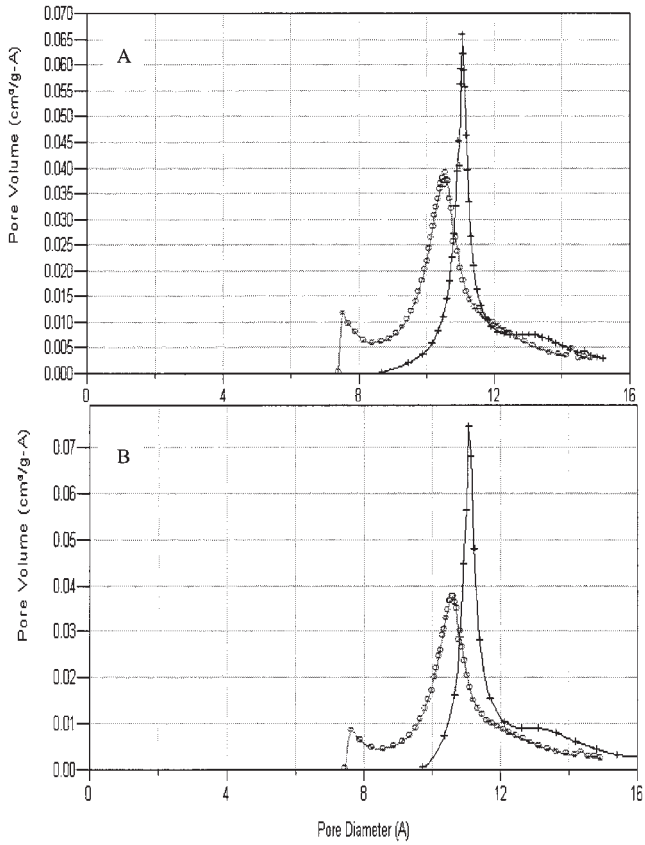

Figure 5. Horvath-Kawazoe differential pore volume plot — cylinder pore geometry (Saito/Foley) with Cheng/Yang correction for small crystallite catalysts (A: (○) CAT-SC-BS and (+) CAT-SC), and large crystallite catalysts (B: (○) CAT-LC-BS and (+) CAT-LC) from nitrogen isotherms.

expected of the magnitude of the faujasite's supercage (~1.2 nm). Given this uncertainty with nitrogen pore-size distribution calculations, a similar analysis using argon adsorption isotherms was carried out.

Figure 6 shows the pore-size distribution assessed from the argon isotherms gathered in samples corresponding to small and large crystallite catalysts, before and after steaming treatment. As shown in Figure 6, a single peak was observed at a pore dia. of ~1.24 nm for small and large crystallite catalysts without steaming treatment (void circle), which value is representative of the supercage diameter of faujasite-type zeolites.

Table 3. Values of the Physical Properties Used in Micropore Size Distribution Calculations

Parameter	Adsorbate		Adsorbent
	N_2	Ar	USY Zeolite◆
Diameter (nm)	0.300*	0.295	0.304
Polarizability (cm^3)	$1.760\ 10^{-24}$ ◆	$1.63\ 10^{-24}$ §	$8.50\ 10^{-25}$
Magnetic susceptibility (cm^3)	$3.600\ 10^{-29}$ ◆	$3.22\ 10^{-29}$	$1.94\ 10^{-29}$
Density per unit area (molecules/cm^2)	$6.7\ 10^{14}$ *	$7.608\ 10^{14}$	$3.75\ 10^{15}$

*Values of parameters for the micropore size distributions (PSD) were obtained following the Horvath-Kawazoe approach.[40]
‡Cheng and Yang.[61]
◆ASAP 2010 Manual, Micromeritics Inc., 1995.

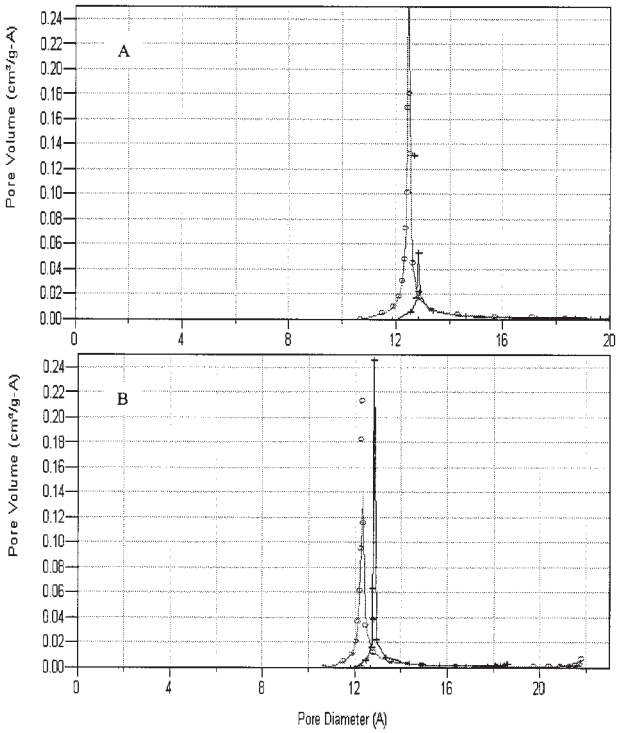

Figure 6. Horvath-Kawazoe differential pore volume plot - Cylinder pore geometry (Saito/Foley) with Cheng/Yang correction for small crystallite catalysts (A: (○) CAT-SC-BS and (+) CAT-SC) and large crystallite catalysts (B: (○) CAT-LC-BS and (+) CAT-LC) from argon isotherms.

However, this peak shifted to 1.27 nm for steamed catalysts (crosses in Figure 6). The slight increase in the location of this peak in the pore-size distribution curve can be attributed to the changes in physical structure and chemical composition accompanying dealumination of Y zeolites.[42] Similar observations in the modification of pore diameter have been reported in the technical literature.[24] Fernández et al.[43] postulated that zeolites have micropores of uniform sizes and super-micropores (0.7-2 nm) and/or mesopores can be created depending on the dealumination conditions.

In order to confirm the shift in the median pore diameter between catalyst samples before and after the steaming treatment, pore-size distributions were obtained from the density functional theory (DFT), and are shown in Figure 7. Similar to the results from the Horvath-Kawazoe model, the DFT provides two-pore diameter (1.17 and 1.5 nm) for catalysts with steaming treatment, even though these methods result from different theoretical considerations. Although the DFT predicts two-pore sizes for steamed catalysts, an acceptable agreement was observed between both the Horvath-Kawazoe model and the density functional theory in regards to the effect of the steaming treatment in the increase of the median pore size.

Catalytic experiments

The catalytic conversion of 1,2,4-trimethylbenzene (1,2,4-TMB) on USY zeolite catalysts can be described on the basis of the reaction network shown in Figure 8. The reactant 1,2,4-TMB undergoes both isomerization and disproportionation reactions leading to the formation of isomers of xylene, trimethylbenzene (TMB) and tetramethylbenzene (TeMB), which are all considered the primary products.

The chemical transformation of trimethylbenzene molecules on USY zeolite catalysts follows a series of steps starting with transport of reactants from the bulk phase to the external catalyst pellet surface. The reactants diffuse inside the pellet macropores toward the individual USY zeolite crystals. The mesopores generated by steaming in these crystallites ensure an optimal accessibility and transport of reactants. This diffusion through the macropore and mesopore is governed by molecular or Knudsen diffusion and does not contribute to selectivity for the kinetically controlled isomerization and disproportionation reactions described in this study. Furthermore, the reactant alkylaromatics physisorb into the micropores of the crystal lattice. Subsequently, the reactant alkylaromatics migrate to the active sites where catalytic transformations take place. There is a restricted molecular transport rate inside the zeolite crystal, induced by the similarity between the size of the involved hydrocarbons and the micropore diameter. Accordingly, the migration of hydrocarbons through the micropores of a zeolite occurs in close contact with the micropore walls. The values for zeolite intracrystalline diffusion coefficients are, therefore, several orders of magnitude lower than those for the molecular and Knudsen diffusion regimes that are typically displayed in meso- and macroporous media.[44,25] Therefore, this study focus on the potential limiting effect of intracrystalline diffusion on both the conversion-level and selectivity.

Figure 9 shows the distribution of primary and secondary products for the 1,2,4-TMB catalytic conversion on CAT-SC at 450°C, residence times of 3, 5 and 7 s, and catalysts/reactant ratio = 5. Under these reaction conditions, there is competition

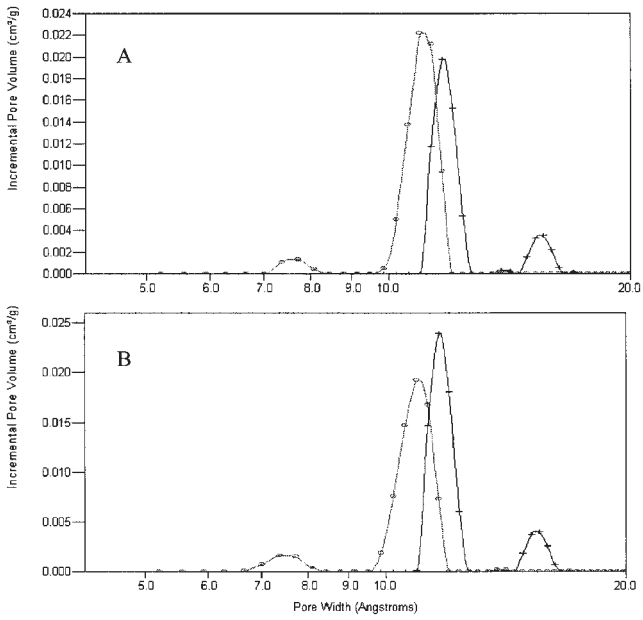

Figure 7. Incremental pore volume using the DFT for small crystallite catalysts (A: (○) CAT-SC-BS and (+) CAT-SC) and large crystallite catalysts (B: (○) CAT-LC-BS and (+) CAT-LC) from nitrogen adsorption isotherms.

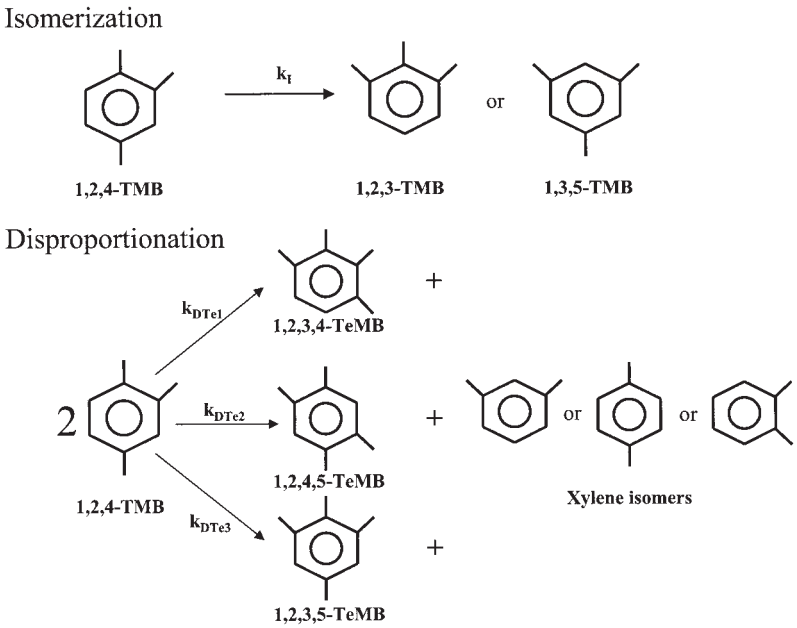

Figure 8. Network of primary reactions for the catalytic conversion of 1,2,4-trimethylbenzene on USY zeolite catalysts.

between isomerization and disproportionation reactions with disproportionation products (TeMB and xylene isomers) being more abundant than the isomerization products (TMB isomers).

Selectivity of 1,2,4-TMB Disproportionation Reactions

One of the objectives of this manuscript is to validate the key role that the USY zeolite pore network plays in governing the selectivity of the 1,2,4-TMB disproportionation toward the tetramethylbenzene isomers.

The theoretical molar ratio of xylene and TeMB produced is one (1), as it can be inferred by the stoichiometry of the 1,2,4-TMB disproportionation reactions shown in Figure 8. However, the experimental results indicated that this molar ratio between xylene and TeMB was above 1 for all the operating conditions considered in this study. Excluding the two products of secondary disproportionation reactions, the higher molecular weight product (TeMB) was consistently present in smaller amounts than the corresponding lower molecular weight product (xylene), as shown in Figure 10. As claimed by Atias et al.[36] the excess of xylene isomers observed can be the result of TeMBs trapped in micropores as coke precursor or consumed in consecutive reactions.

Figure 10 compares the distribution of disproportionation

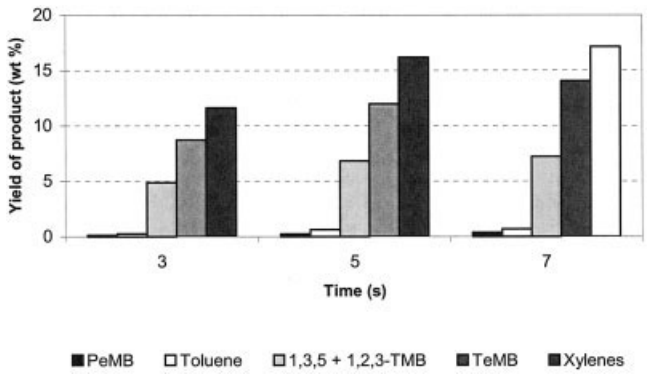

Figure 9. Distribution of primary and secondary products in the 1,2,4-TMB conversion on CAT-SC catalyst at Catalyst/1,2,4-TMB ratio = 5 and temperature = 450 °C.

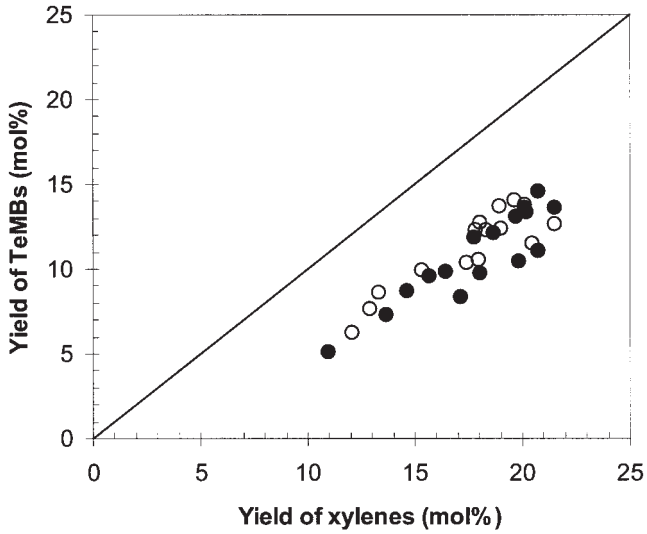

Figure 10. Disproportionation products during 1,2,4-TMB catalytic conversion on (●) CAT-LC and (○) CAT-SC.

Reaction conditions: Catalyst/1,2,4-TMB ratio = 5 (wt/wt), reaction times = 3, 5 and 7s, and temperature = 350, 400, 450, 500, and 550 °C:

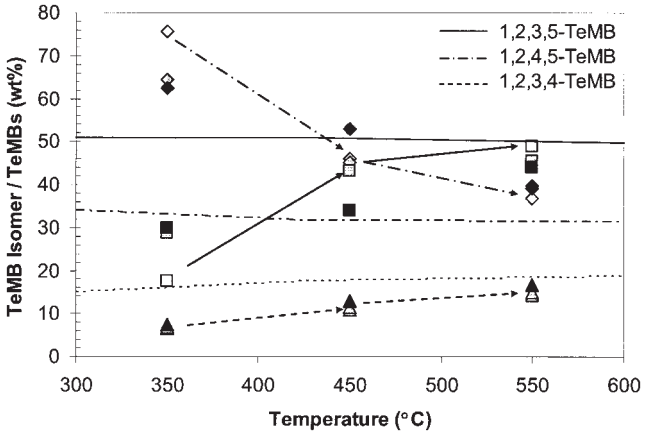

Figure 11. Influence of temperature on the TeMB isomer distribution during the catalytic conversion of 1,2,4-TMB on CAT-SC (Catalyst/1,2,4-TMB = 5).

Residence time = 3 s (white symbols); 5 s (gray symbols); 7 s (black symbols), (◇) 1,2,4,5-TeMB; (≤) 1,2,3,5-TeMB; (ρ) 1,2,3,4-TeMB. Equilibrium values[58] are represented with continuous lines.

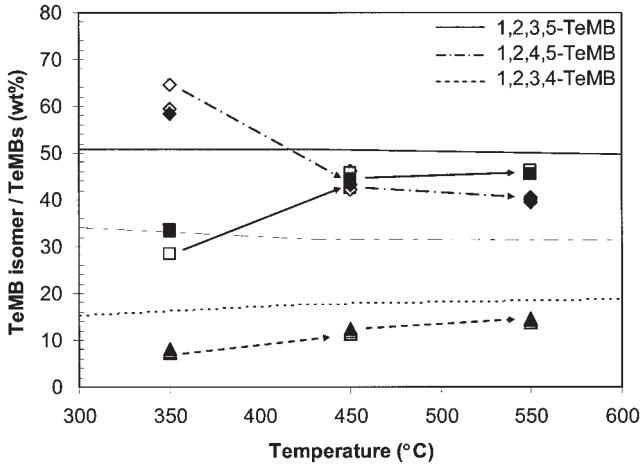

Figure 12. Influence of temperature on the TeMB isomer distribution during the catalytic conversion of 1,2,4-TMB on CAT-LC (Catalyst/1,2,4-TMB = 5).

Residence time = 3 s (white symbols); 5 s (gray symbols); 7 s (black symbols) (◇) 1,2,4,5-TeMB, (≤) 1,2,3,5-TeMB; (ρ) 1,2,3,4-TeMB. Equilibrium values[58] are represented with continuous lines.

products attained in both CAT-SC and CAT-LC and displays disproportionation products ratios larger than one ((mol xylenes)/(mol TeMB) > 1). It can be observed that the crystallite size does not have an apparent effect in the distribution of the tetramethylbenzene and xylene isomers. This result indicates that the geometric characteristics (a) of the diffusion path of reactant molecules while being transported toward the active centers (reactant selectivity), or (b) of disproportionation product molecules (xylene and TeMBs) while evolving toward the external surface of the crystallites (product selectivity) do not play a significant role in catalyst selectivity.

Among the TeMB isomers, the most desirable product is the 1,2,4,5-isomer called durene, which can be oxidized to pyromellitic anhydride (raw material for heat-resisting polymers). As the 1,2,3,5-isomer is thermodynamically the most stable among TeMBs, the production of durene requires the development of shape-selective catalysts.

Figures 11 and 12 report the TeMB isomer distribution in the catalytic conversion of 1,2,4-TMB on CAT-SC and CAT-LC, respectively. The distribution of TeMBs at low temperatures (~350°C) shows that the 1,2,4,5-TeMB is produced more abundantly than expected from thermodynamic equilibrium whereas the other two isomers: 1,2,3,5-TeMB and 1,2,3,4-TeMB are below their respective equilibrium values. Moreover, at low-temperature (~350°C) both catalysts present similar 1,2,3,4- and 1,2,3,5-TeMB selectivity, whereas the 1,2,4,5-TeMB selectivity is larger for the case of CAT-SC. At higher temperatures (~550°C), even though 1,2,4,5-TeMB is still produced more abundantly than expected from thermodynamic equilibrium, both catalysts show similar activity and selectivity with all TeMB isomers approaching values at equilibrium. In conclusion, small crystallite USY zeolite catalysts and low temperatures favor the production of 1,2,4,5-TeMB, which is the smallest among the TeMB isomers (Table 4). This experimental finding is in line with results obtained elsewhere. Kikuchi and coworkers[45] proposed an alkylation-type mechanism under the restricted space conditions of micropores and claimed that disproportionation may promote 1,2,4,5-TeMB vs. the others TeMBs, given its lower minimum van der Waals diameter (Table 4). TeMB distribution on USY catalysts falls in the category of shape-selectivity where there is an alteration of the thermodynamic equilibrium favoring the formation of 1,2,4,5-TeMB over the other isomers. Depending on the disproportionation mechanism, the selective formation of 1,2,4,5-TeMB relative to 1,2,3,4- and 1,2,3,5-TeMB might be interpreted as a transition-state or product shape selectivity effect.[46]

One initial explanation advanced to justify the results of this study was to relate the change in TeMB distribution with temperature to the crystallite size arguing about a possible influence of product-diffusion constrains. However, this possibility is discarded in the upcoming sections given that restricted transition-state selectivity is proven as a more sound explanation.

A generally accepted disproportionation mechanism of alkylaromatics involves a byphenylic transition-state intermedi-

Table 4. Minimum van der Waals Diameters for Some Alkylbenzenes

Alkylbenzenes	Minimum van der Waals Diameter (nm)
p-xylene	0.67
m-xylene	0.74
o-xylene	0.74
1,2,3-trimethylbenzene	0.79
1,2,4-trimethylbenzene	0.74
1,3,5-trimethylbenzene	0.86
1,2,3,4-tetramethylbenzene	0.79
1,2,3,5-tetramethylbenzene	0.86
1,2,4,5-tetramethylbenzene	0.74
1,3,5-triethylbenzene	0.92
1,3,5-triisopropylbenzene	0.94

Source: Gnep et al.[56]; Satterfield and Cheng.[57]

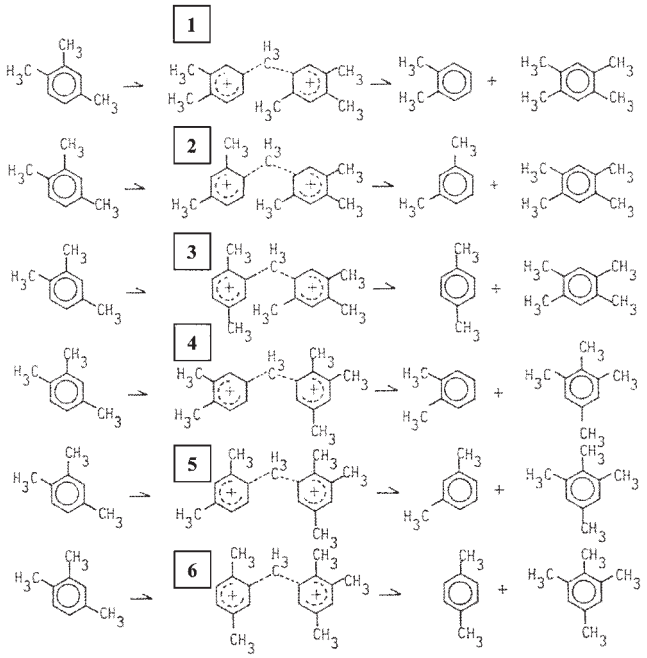

Figure 13. Bimolecular mechanism postulated for the disproportionation of 1,2,4-TMB.[45]

ate as proposed by Csicsery[47,48] for the transalkylation of alkylbenzenes over mordenite catalysts. Among the possible transition-state intermediates in the disproportionation of 1,2,4-TMB, the formation of the more linear transition-state intermediate is more sterically favored in the micropore structure. Figure 13 bimolecular transition states to yield 1,2,4,5-TeMB, 1,2,3,5-TeMB and xylene isomers. Figure 13 shows that the intermediates that are more linear (cases 1, 2 and 3) yield the 1,2,4,5-TeMB isomer. Therefore, the tetramethylbenzenes distribution may be justified on the basis of the restricted transition-state selectivity concept.

Modeling of Catalytic Conversion of 1,2,4-TMB on USY Zeolite Catalysts

The catalytic conversion of 1,2,4-TMB in the CREC riser simulator can be described by a set of equations involving the various catalytic rates of isomerization and disproportionation reactions shown in Figure 8. This study expands the model proposed by Atias et al.[36] and breaks down the disproportionation reaction into three parallel reactions producing the three TeMB isomers, respectively. This proposed kinetic model, which considers apparent kinetic parameters, complements the experimental findings and gives insights into the catalyst selectivity.

Considering high gas mixing,[49] intense fluidization, and uniform temperature displayed in the CREC Riser Simulator, this laboratory reactor can be modeled as an ideal batch reactor by the following equation

$$\frac{V}{W_{cr}}\frac{dC_i}{dt} = r_i \tag{1}$$

where V is the volume of the reactor, W_{cr} is the weigh of USY zeolite crystallites supported on the catalyst, C_i is the gas phase concentration of species i and r_i is the observed reaction rate of species i.

The material balance expressed by Eq. 1 can be written in terms of the various species considered in the network of reactions (Figure 8): 1,2,4-TMB (A); 1,2,3-TMB (B); 1,3,5-TMB (C); 1,2,3,4-TeMB (Te1); 1,2,4,5-TeMB (Te2); 1,2,3,5-TeMB (Te3); and xylenes (X)

$$-\frac{V}{W_{cr}}\frac{dC_A}{dt} = k_I C_A \varphi^I_{\text{int}} + 2(K_{DTe1} + k_{DTe2} + k_{DTe3})C_A^2 \varphi^D_{\text{int}} \tag{2}$$

$$-\frac{V}{W_{cr}}\frac{d(C_B + C_C)}{dt} = -k_I C_A \varphi^I_{\text{int}} \tag{3}$$

$$-\frac{V}{W_{cr}}\frac{dC_{Te1}}{dt} = -k_{DTe1} C_A^2 \varphi^D_{\text{int}} \tag{4}$$

$$-\frac{V}{W_{cr}}\frac{dC_{Te2}}{dt} = -k_{DTe2} C_A^2 \varphi^D_{\text{int}} \tag{5}$$

$$-\frac{V}{W_{cr}}\frac{dC_{Te3}}{dt} = -k_{DTe3} C_A^2 \varphi^D_{\text{int}} \tag{6}$$

$$-\frac{V}{W_{cr}}\frac{dC_X}{dt} = -(k_{DTe1} + k_{DTe2} + k_{DTe3})C_A^2 \varphi^D_{\text{int}} \tag{7}$$

where k_I and k_{Di} are the kinetic constants corresponding to the reaction network in Figure 8, φ^I_{int} and φ^D_{int} are the deactivation functions for isomerization and disproportionation, respectively. It can be noticed that the isomerization of 1,2,4-TMB is assumed to be first-order, whereas the disproportionation is adopted to follow a second-order kinetics, as proposed by Kikuchi et al.[45] and Ko and Kuo.[50]

To develop this kinetic model, it was assumed that reactant molecules diffuse into the catalyst matrix reaching the external surface of the zeolite crystallites. These diffusing molecules are alleged to display negligible transport limitations around the 60 μm pellets (intense gas mixing) and inside the inert porous matrix (mesoporous network). Thus, these molecules were considered to reach the external surface of the USY crystallites displaying no-diffusional limitations. Furthermore, it was proven by Atias et al.[23] that 1,2,4-TMB reactant molecules do not display intracrystalline diffusion limitations, therefore, the overall reaction rate can be considered equivalent to the intrinsic reaction rate.

Equation 1 also assumes that catalytic isomerization and disproportionation of 1,2,4-TMB occur solely in the zeolite crystallites with the catalyst matrix being inert to reaction. Moreover, this model takes into account catalytic reactions and neglects thermal conversion, which was found to have a small contribution in the total conversion of 1,2,4-TMB at the operating conditions of this study.

The kinetic constants are function of temperature and can be

expressed using the Arrhenius equation and a centering temperature, $T_0 = 450°C$, as follows

$$k_I = k_{I,0}\exp\left[-\frac{E_I}{R}\left(\frac{1}{T}-\frac{1}{T_0}\right)\right] \quad (8)$$

$$k_{Di} = k_{Di,0}\exp\left[-\frac{E_{Di}}{R}\left(\frac{1}{T}-\frac{1}{T_0}\right)\right] \quad (9)$$

where $k_{I,0}$ and $k_{Di,0}$ are pre-exponential factors, and E_I and E_{Di} are the activation energies for isomerization and disproportionation reactions, respectively. The deactivation functions are based on the reactant conversion model,[51] and can be expressed as follows

$$\varphi^I_{\text{int}} = \exp(-\lambda^I(y_B + y_C)) \quad (10)$$

$$\varphi^D_{\text{int}} = \exp(-\lambda^D y_X) \quad (11)$$

with λ^I and λ^D representing the deactivation parameters for isomerization and disproportionation reactions, respectively, and y_i the mass fraction of species i defined by the following equation

$$y_i = \frac{C_i VMW_i}{m_{HC}} \quad (12)$$

where MW_i is the molecular weight of species i and m_{HC} is the total mass of reactant injected.

From all the above, the catalytic conversion of 1,2,4-TMB on USY zeolite catalysts can be mathematically modeled by the system of six partial-differential equations formulated by Eqs 2 to 7. This system of partial differential equations contains ten (10) unknown parameters, $k_{DTe2,0}$; E_{DTe2}; $k_{DTe3,0}$; E_{Te3}; $k_{DTe1,0}$; E_{Te1}; $k_{I,0;}$ E_I; λ_I; and λ_D, which are assessed employing nonlinear regression techniques. The experiments for this chemical system were carried out in the CREC riser simulator at temperatures in the range of 350–550°C and reaction times 3; 5 and 7 s. Because experimental data were available for all six dependent variables: C_A, $C_B + C_C$, C_{Te1}, C_{Te2}, C_{Te3}, and C_X, multiple nonlinear regression was performed by simultaneously fitting all six equations to the data. The technique for minimization of the sum of squared residuals is the large-scale algorithm based on the interior-reflective Newton method described in Coleman and Li.[52]

The results of the nonlinear regression of parameters and statistical analysis are shown in Table 5. Individual parameter 95%-confidence intervals were calculated and showed the soundness of the mathematical model proposed. Moreover, the extent of the correlation between parameters was calculated and shown in the matrix of correlation coefficients (Table 6). The correlation coefficients indicated the low degree of correlation between the kinetic parameters assessed, which is another indication of the soundness of the proposed model to predict the data. However, it was found that the deactivation parameters for both isomerization and disproportionation reactions displayed a somewhat significant correlation with other kinetic parameters.

Table 5. Parameter Values and 95%-Confidence Intervals Obtained from the Nonlinear Regression and the Statistical Analysis of Experimental Data

Parameter	Value	95%-Confidence Intervals	
		Lower Value	Upper Value
$k_{DTe2,0}$ (m^6/[mol(kg of crystallite)s])	0.345	0.262	0.428
E_{DTe2} (kJ/mol)	2.08	0.953	3.20
$k_{DTe3,0}$ (m^6/[mol(kg of crystallite)s])	0.312	0.237	0.388
E_{Te3} (kJ/mol)	5.16	3.84	6.47
$k_{DTe1,0}$ (m^6/[mol(kg of crystallite)s])	0.142	0.101	0.184
E_{Te1} (kJ/mol)	5.24	2.51	7.97
$k_{I,0}$ (m^3/[(kg of crystallite)s])	0.0257	0.0	0.0640
E_I (kJ/mol)	15.8	7.03	24.7
$\lambda^I(-)$	27.7	5.41	49.9
$\lambda^D(-)$	6.08	3.42	8.74

The regressed parameters for activation energies indicate that among the TeMBs, the 1,2,3,4-TeMB and the 1,2,3,5-TeMB display larger activation energies than the one for 1,2,4,5-TeMB: 5.24-5.16 kJ/mol versus 2.08 kJ/mol, respectively. These reported values represent apparent activation energies, which include the effects of the intrinsic kinetic catalytic reaction and the adsorption of the reactant.[35] Even though a comparison between these values and the ones found in the technical literature have to be done cautiously, the activation energies of this study are in the same order of magnitude to values found in the technical literature for the catalytic transformation of alkylbenzenes on large pore zeolite.[47] The activation energies reported in this study indicate a preferential formation of activated complexes leading to 1,2,4,5-TeMB, and this is consistent with the molecular modeling of probe molecules interacting with the USY zeolite framework discussed in following sections.

Molecular Modeling and Analysis of the interaction between the "relaxed" USY zeolite and molecules

Figure 2 shows the "relaxed" and "nonrelaxed" USY zeolite structure modeled in this study, taken into account PSDs obtained experimentally. The "nonrelaxed" window had a characteristic window opening of 0.74 nm, whereas the "relaxed" window had an opening equals to 0.81 nm (PSD found experimentally using N_2 and Ar isotherm).

Performing molecular simulation with the"relaxed" USY zeolite window (Figure 2B), and a probe molecule provides insights into the interactions occurring when a molecule is diffusing into a supercage. Taking into consideration that the guest molecule-host structure energy arises mainly from steric requirements, minimum steric energies were calculated by placing the probe molecule in the optimum position at the center of the USY zeolite window model. Furthermore, the probe molecule's configuration was modified in order to produce energy-minimized structures.

Experimental and theoretical results of this study can be explained taken into account that the proposed model corresponds to a rigid framework. Auerbach et al.[53] indicated that the direct examination of the influence of zeolite vibrations on guest dynamics suggests a strong influence on the activated diffusion of tight-fitting guest-zeolite systems. These authors pointed out that for tight-fitting host-guest systems, the frame-

Table 6. Matrix of Correlation Coefficients for the Nonlinear Regression of Parameters

	$k_{DTe2,0}$	E_{DTe2}	$k_{DTe3,0}$	E_{DTe3}	$k_{DTe1,0}$	E_{DTe1}	$k_{I,0}$	E_I	λ^I	λ^D
$k_{DTe2,0}$	1	0.2104	0.8445	0.1167	0.6557	0.05648	−0.3221	−0.2987	−0.318	0.9304
E_{DTe2}		1	0.1052	−0.1429	0.07573	−0.2236	0.06499	0.01395	0.06614	0.103
$k_{DTe3,0}$			1	0.08549	0.6411	0.0821	−0.3183	−0.2913	−0.3137	0.9215
E_{DTe3}				1	0.1317	−0.2498	0.06447	0.01066	0.06181	0.1127
$k_{DTe1,0}$					1	−0.0268	−0.2641	−0.2341	−0.2538	0.7561
E_{DTe1}						1	0.03506	−0.0168	0.03278	0.05917
$k_{I,0}$							1	0.9385	0.9916	−0.436
E_I								1	0.9476	−0.4137
λ^I									1	−0.4397
λ^D										1

work vibrations must allow for an accurate treatment of the activation energy for molecular jumps through flexing channels and/or windows. Nonetheless, calculations performed in this study with "relaxed" and "nonrelaxed" models allow concluding that a minor increase of the window diameter (consequence of steaming treatment, as described earlier) modifies significantly the diffusional properties of the molecules such as TMBs. This assessment can be developed in terms of a relative steric energy ($\Delta E = E1 - (E2+E3)$). This relative steric energy (ΔE) involves the difference of the following two terms (refer to Table 7): (a) Steric energy when the probe molecule is placed inside the cage (final stage), and (b) Steric energy of the molecule when this probe molecule is far away from the cage plus the steric energy of the window itself (initial stage). The ΔE change of steric energy from the initial to the final stage provides information about the ease of reaching different conformational situations. Even more, this relative steric energy represents the difficulty of the probe molecule to access the inner cage, and can provide trends in activation energies for the intracrystalline diffusion of the probe molecule into the zeolite supercage.

Table 7 shows the steric energies corresponding to the interaction of the "relaxed" window model (0.81 nm) with different probe molecules. In the molecular simulation using 1,2,4-TMB as the probe molecule, the relative steric energy (-58.2 kJ/mol) indicated no restrictions in terms of accessibility into the USY zeolite micropores. This finding supports the work of Atias et al.[36] who studied the catalytic conversion of 1,2,4-TMB on USY zeolite catalysts of various crystallite sizes in a range of temperature = 350–550°C and catalyst/(1,2,4-TMB injected) ratio = 5. These authors found that the catalytic reaction of 1,2,4-TMB under those operating conditions was not hindered by intracrystalline diffusion.

In contrast, results of molecular simulation for 1,2,4-TMB as the probe molecule in a 0.74 nm window structure showed that the relative steric energy to reach the supercage was ~62 kJ/mol. This value is positive and higher than the one observed for the 0.81 nm window model.

Calculations of steric interaction energies for the TeMB isomers do not show significant differences, which indicated that the mobility of these molecules through the USY zeolite pore network was not hindered by physical constraints. Moreover, comparing the relative steric energies of 1,2,4-TMB (-58.2 kJ/mol) with the ones for TeMBs (-70 to -50 kJ/mol) leads to similar conclusions (refer to Table 7). Therefore, product shape selectivity cannot explain the changes in thermodynamic equilibrium for the disproportionation of 1,2,4-TMB favoring the production of 1,2,4,5-TeMB.

Similar molecular simulation studies were carried out selecting probe molecules used in a previous work by our research group,[54] based on the catalytic conversion of 1,3,5-triisopropylbenzene (1,3,5-TIPB), and 1,3-diisopropylbenzene (1,3-DIPB) on FCC catalysts (CAT-SC and CAT-LC). The purpose was to corroborate the validity of the methodology employed in this manuscript with regards to tetramethylbenzene isomers distribution. The interactions of these two probe molecules: 1,3,5-TIPB and 1,3-DIPB with the "relaxed" USY window models were evaluated. Results are also shown in Table 7. A negative relative steric energy of -137.7 kJ/mol was assessed for 1,3-DIPB, and supported the experimental data indicating that the catalytic conversion of this molecule on FCC catalysts was controlled by the intrinsic reaction and it did not display diffusion restrictions. For the case of the catalytic cracking of 1,3,5-TIPB on USY catalysts, the results of the molecular simulation corroborated the significant mobility restrictions and diffusion limitations displayed by this molecule.[54] Table 7 shows a positive relative steric energy for the 1,3,5-TIPB-"relaxed" window model of +951.9 kJ/mol, which indicates

Table 7. Absolute and Relative Steric Energies Found of the Probe Molecule-"Relaxed" USY Zeolite Window Model Using MM2 Method

	Absolute Steric Energy (kJ/mol)		Relative Steric Energy (kJ/mol)
Probe Molecule	Final Stage: E_1	Initial Stage: E_2*	$\Delta E = E_1 - E_2$
1,2,4-TMB	3491.1	3549.3	−58.2
1,3,5-TIPB	4531.3	3579.4	951.9
1,3-DIPB	3429.6	3567.3	−137.7
1,2,3,4-TeMB	3492.0	3562.3	−70.3
1,2,3,5-TeMB	3489.9	3555.1	−65.3
1,2,4,5-TeMB	3497.0	3551.0	−54.0

*Absolute steric energy of the "relaxed" window (0.81 nm) = 3558.5 kJ/mol.
Final Stage: Probe molecule located at the window.
Initial Stage: Probe molecule apart (~0.6 nm) from the window.

Table 8. Molecular Dimensions and Connolly Parameters of the Various Transition States for the Formation of TeMBs from the Disproportionation of 1,2,4-TMB

Transition State[1]	D^2 (nm)	Connolly Accessible Surface Area (nm^2)	Connolly Molecular Surface Area (nm^2)	Connolly Excluded Volume (nm^3)	Relative Steric Energy (kJ/mol)
1	1.19	5.20	2.85	0.257	4.3
2	1.16	5.18	2.84	0.256	−2.1
3	1.07	5.06	2.78	0.258	0.4
4	1.20	5.34	2.89	0.256	3.8
5	1.14	5.33	2.88	0.255	−0.1
6	1.07	5.24	2.92	0.259	−2

[1]For keys refer to Figure 13.
[2]Maximum distance considering substituents in the transition state.

the highly restricted mobility of this molecule, well in agreement with the experimental findings.

Molecular Simulation of Transition states for TeMB Formation

Once the molecular simulation using the MM2 method showed that product-shape selectivity could not explain the distribution of tetramethylbenzene isomers, complementary studies, based on the transition states for TeMB formation were carried out. The implementation of the MOPAC method described in previous sections was required given a proposed transition state on the probe molecules in order to elucidate if the TeMB distribution obtained in the catalytic conversion of 1,2,4-TMB can be explained in terms of transition-state selectivity.

The VdW diameters are useful as a first insight, whereas the Connolly areas are more complete in the definition of the available space occupied by the molecules. In this sense, these parameters are more adequate to establish the real space occupied by a molecule.[55] Table 8 reports three Connolly molecular parameters for transition states of TeMBs (forms 1 to 6 as depicted in Figure 13). The "Connolly Accessible Area" represents the locus of the center of a probe sphere (representing a solvent) as it is rolled over the molecular shape. The "Connolly Molecular Surface Area" and the "Connolly Solvent Excluded Volume" represent the contact surface created when the same probe sphere is rolled over the molecular shape and the volume contained within the contact molecular surface, respectively (Figure 14).

The molecular parameter "D" in Table 8 is the maximum linear distance considering the substitutes in the transition state. The significance of this parameter can be established using as a basis a 1.2 nm dimension that represents the space available inside the supercage. Transition states with high values of D are less probable to occur. Table 8 also reports three Connolly molecular parameters for the transition states of TeMB (forms 1 to 6 as shown in Figure 13). Comparison between these parameters provides the basis to evaluate the molecular dimensions, and to relate them with the steric constraints and the proposed mechanism/locations of these reactions. Obviously, the transition states that are more voluminous find more steric difficulties for their formation inside the supercage. The relative steric energy shown in Table 8 was calculated as the difference in steric energy between the dimeric conformer and two molecules of 1,2,4 TMB. This calculation assesses the steric energy needed for the formation of the dimeric conformer inside the supercage, starting from two individual molecules far away from each other and apart from the supercage and provides a qualitative evaluation of the ease of formation among conformers with the same atom number.

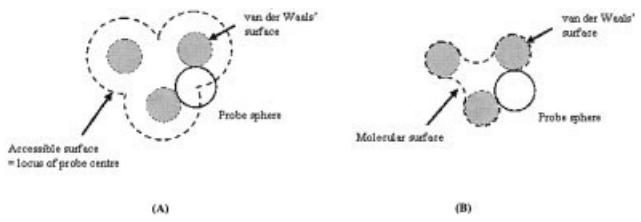

Figure 14. Representation of the accessible surface of a molecule (A), and the molecular surface of a molecule (B).

The results obtained from this molecular simulation are shown in Table 8 and can be summarized as follows:

1. In terms of the magnitude of Connolly surface accessible area, the observed ordering is:

Form 3 < Form 2 < Form 1 < Form 6 < Form 5 < Form 4

2. Transition-states 1, 2 and 3, which lead to the formation of 1,2,4,5-TeMB, display the lower Connolly molecular surface area out of the six transition states analyzed

3. Relative steric energies of the various probe molecules shown in Table 7 using the "relaxed" USY zeolite window are in the -138 to +952 kJ/mol range, whereas the relative steric energies of the transition states shown in Table 8 are in the range of -2 to 4 kJ/mol.

4. Transition states for the TeMB isomers showed slight differences in their relative steric energies, however, differences in the molecular Connolly parameters are significant. For instance, transition state 5 (for 1,2,3,5 TeMB) shows a relative steric energy of -0.1 kJ/mol and a small dimeric conformer distance D of 1.14 nm, but its Connolly accessible surface area is one of the largest (5.33 nm^2) among the six transition-states studied.

Consequently, the applicability of a restricted transition-state shape-selectivity concept can be established studying the experimental distribution of TeMB isomers, where 1,2,4,5-TeMB (produced from the transition-states 1, 2, and 3) is the most sterically favored. As described by the Connolly, accessible surface area and molecular surface area parameters, the transition states promoted in the 1,2,4-TMB disproportionation on USY catalyst lead predominately to the production of 1,2,4,5-

TeMB whereas the rest of the TeMB isomers present more sterically-restricted transition states that hinder their formation.

Conclusions

(a) Pore-size distribution measurements show that hydrothermal treatment of FCC catalysts enlarges the USY zeolite windows.

(b) Reaction experiments in a fluidized CREC riser simulator allow establishing kinetic parameters and energies of activation for both the isomerization and disproportionation steps. The activation energy for 1,2,4,5-TeMB-formation display the lowest value suggesting that the transition state for this isomer is the less energetically demanding, and as a result this path is favored.

(c) Transition state shape-selective on USY zeolite crystallites is a relevant factor to explain TeMB isomer product distribution under conditions where pore configuration of USY zeolite constrains the formation of transition-state species and leads to the production of 1,2,4,5-TeMB surpassing isomer chemical reaction equilibrium distributions.

Acknowledgments

This work was supported with funding from the Universidad Nacional del Sur, the Consejo Nacional de Investigaciones Científicas y Técnicas (CONICET), and the Natural Sciences and Research Council of Canada (NSRCC).

Notation

C_i = gas-phase concentration of species *I,* mol/cm^3
E_I = activation energies for isomerization reaction, kJ/mol
E_{Di} = activation energies for disproportionation reactions, kJ/mol
E_1 = absolute steric energy of the window-molecule system when probe molecule is located at the window, kJ/mol
E_2 = Absolute steric energy of the window-molecule system when probe molecule is apart (~6Å) from the window, kJ/mol
k_I = kinetic constant for isomerization reaction, m^3/[(kg of crystallite) s]
$k_{I,0}$ = pre-exponential factor for isomerization reaction, m^3/[(kg of crystallite) s]
k_{Di} = kinetic constants for disproportionation reactions, m^6/[mol (kg of crystallite) s]
$k_{Di,0}$ = pre-exponential factor for disproportionation of 1,2,4-TMB, m^6/[mol (kg of crystallite) s]
MW_i = molecular weight of species *I,* g/mol
m_{HC} = total mass of reactant injected in the experimental reactor, 0.162 g
R = ideal gas constant, 8.314 J/mol K
r_i = reaction rate of species *I,* mol/[(kg of crystallite) s]
T = temperature, K
t = time, s
T_0 = centering temperature, 450°C
V = volume of the experimental reactor, 52 cm^3
W_{cr} = weight of USY zeolite crystallites (supported on the catalyst) loaded in the experimental reactor 0.243 g
y_i = mass fraction of species *I,* wt/wt

Greeks letters

ΔE Relative steric energy of the window-probe molecule system between final (E_1) and initial (E_2) stages of the molecular simulation, kJ/mol
φ^I_{int} = deactivation function for isomerization reaction
φ^D_{int} = deactivation function for disproportionation reactions
λ^{I} = deactivation parameter for isomerization reaction
λ^{D} = deactivation parameter for disproportionation reactions

Subscripts

A = 1,2,4-TMB
B = 1,2,3-TMB
C = 1,3,5-TMB
cr = crystallite
HC = hydrocarbons
i = species
int = intrinsic
I = isomerization reaction
$Te1$ = 1,2,3,4-TeMB
$Te2$ = 1,2,4,5-TeMB
$Te3$ = 1,2,3,5-TeMB
X = xylenes

Literature Cited

1. Corma A., Orchilles AV. Current views on the mechanism of catalytic cracking. *Microporous and Mesoporous Materials*. 2000;35-36:21-30.
2. Avidan AA. FCC is far from being a mature technology. *Oil & Gas J*. 1992;18:59-67.
3. Ying JY. Nanostructural tailoring: Opportunities for molecular engineering in catalysis. *AIChE J*. 2000;46:1902-1906.
4. Leiby S. FCC catalyst technologies expand limits of process capability. *Oil and Gas J*. 1992;23:49-58.
5. Sadeghbeigi R. *Fluid Catalytic Cracking: Design, Operation, and Troubleshooting of FCC Facilities*. Houston: Gulf Publishing Co; 1995.
6. Bhatia S. *Zeolite Catalysis: Principles and Applications*. Boca Raton: CRC Press, Inc; 1990.
7. McDaniel CV, Maher PK. Zeolite stability and ultrastable zeolites. In: Rabo JA. ACS *Monograph: Zeolite Chemistry and Catalysis*. Washington: American Chemical Society, 1976;171:285-331.
8. Choi-Feng C, Hall J, Huggins B, Beyerlein R. Electron microscope investigation of mesopore formation and aluminum migration in USY catalysts. *J of Catalysis.* 1993;140:395-425.
9. Patzelova V, Jaeger N.I. Texture of deep bed treated Y zeolites. Zeolites .1987;7:240-242.
10. Janssen AH, Koster AJ, de Jong KP. On the shape of the mesopores in zeolite Y: a three-dimensional transmission electron microscopy study combined with texture analysis. *J of Phys Chem B*. 2002;106:11905-11909.
11. Klinowski J, Thomas JM, Fyfe CA, Gobbi GC. Monitoring of structural changes accompanying ultrastabilization of faujasitic zeolite catalysts. *Nature*. 1982;296:533-536.
12. Klinowski J, Fyfe CA, Gobbi GC. High-resolution solid-state nuclear magnetic resonance studies of dealuminated zeolite Y. *J of the Chem Soc*. Faraday Transactions1: Physical Chemistry in Condensed Phases. 1985; 8(12):3003-3019.
13. Samoson A, Lippmaa E, Engelhardt G, Lohse U, Jerschkewitz HG. Quantitative high-resolution aluminum-27 NMR: tetrahedral nonframework aluminum in hydrothermally treated zeolites. *Chem Phys Lett*. 1987; 134(6):589-592.
14. Sanz J, Fornes V, Corma A. Extra framework aluminum in steam and tetrachlorosilane-dealuminated Y zeolite: an aluminum-27 and silicon-29 nuclear magnetic resonance study. Faraday Transactions 1. *J of the Chem Soc.* 1988;84:3113-3119.
15. Beaumont R, Barthomeuf D. X, Y, Aluminum-deficient and ultrastable faujasite-type zeolites. I. Acidic and structural properties. *J of Catalysis*. 1972;26:218-225.
16. Janin A, Lavalley JC, Macedo, A, Raatz, F. FT-IR Study of the broensted acid sites in dealuminated HY zeolites using specific probe molecules. In: Flank WH, Whyte TE. ACS Symposium Series; 368. *Perspectives in Molecular Sieve Science*. Washington, DC: American Chemical Society; 1988:117-135.
17. Auroux A, Ben Taarit Y. Calorimetric investigation of the effect of dealumination on the acidity of zeolites. *Thermochimica Acta*. 1987;122: 63-70.
18. Biaglow AI, Parrillo DJ, Kokotailo GT, Gorte RJ. A study of dealuminated faujasites. *J of Catalysis*. 1994;148: 213-223.
19. Chen D, Sharma S, Cardona-Martinez N, Dumesic JA, Bell VA, Hodge GD, Madon, RJ. Acidity studies of fluid catalytic cracking catalysts by microcalorimetry and infrared spectroscopy. *J of Catalysis*. 1992;136: 392-402.
20. Beyerlein RA, Choi-Feng C, Hall JB, Huggins B, Ray GJ. Effect of

steaming on the defect structure and acid catalysis of protonated zeolites. *Topics in Catalysis*. 1997;4:27-42.
21. Miller JT, Hopkins PD, Meyers BL, Ray GJ, Roginski RT, Kuehne MA, Kung HH. Towards understanding the enhanced cracking activity of steamed Y zeolites. *Appl Catalysis A*. 1996;136:29-48.
22. Al-Khattaf S, de Lasa HI. Diffusion and reactivity of hydrocarbon feedstocks in FCC catalysts. *C J of Chem Eng*. 2001;79:329-341.
23. Atias JA, de Lasa HI. Adsorption and catalytic reaction in FCC catalysts using a novel fluidized CREC riser simulator. *Chem Eng Sci*. 2004;59:5663-5669.
24. Kubelkova L, Beran S, Malecka A, Mastikhin V. Acidity of modified Y zeolites: effect of nonskeletal Al, formed by hydrothermal treatment, dealumination with SiCl4, and cationic exchange with Al. *Zeolites*. 1989; 9(1):12-17.
25. Karger J, Ruthven D. *Diffusion in Zeolites and Other Microporous Solids*. New York: John Wiley & Sons, Inc;1992.
26. Kung H, Williams B, Babitz S, Miller J, Snurr R. Towards understanding the enhanced cracking activity of steamed Y zeolites. *Catalysis Today*. 1999;52:91-98.
27. Smit B, Krishna R. Molecular simulations in zeolitic process design. *Chem Eng Sci*. 2003;58:557-568.
28. Tonetto G, Atias JA, Lasa HI. FCC Catalysts with different zeolite crystallite sizes: acidity, structural properties and reactivity. *Appl Catalysis A*. 2004;270:9-25.
29. Topsøe NY, Pedersen K, Derouane E. Infrared and temperature-programmed desorption study of the acidic properties of ZSM-5-type zeolites. *J of Catalysis*. 1981;70:41-52.
30. Maache M, Janin A, Lavalley J. Acidity of zeolites beta dealuminated by acid leaching: an FTIR study using different probe molecules (pyridine, carbon monoxide). *Zeolites*. 1993;13:419-426.
31. Rosenthal D, White M, Parks G. Estimating the relative acid site density of silica-alumina by infrared spectroscopy using a selective reactant poison. *AIChE J*. 1987;33:336-340.
32. Emeis C. Determination of integrated molar extinction coefficients for infrared absorption bands of pyridine adsorbed on solid acid catalysts. *J of Catalysis*. 1993;141:347-354.
33. Jaroniec M, Kruk M, Olivier JP, Koch S. A New Method for the Accurate Pore Size Analysis of MCM-41 and other Silica Based Mesoporous Materials. In: Unger KK, Kreysa G, Baselt JP. *Studies in Surface Science and Catalysts*, *128 (Characterization of Porous Solids V)*. Amsterdam: Elsevier; 2000;128:71-80.
34. Occelli M, Olivier J, Auroux A. The location and effects of coke deposition in fluid cracking catalysts during gas oil cracking at microactivity test conditions. *J of Catalysis*. 2002;209:385-393.
35. de Lasa H. Riser simulator for catalytic cracking studies. U.S. Patent #5,102,628. 1992.
36. Atias JA, Tonetto G, de Lasa HI. Catalytic conversion of 1,2,4-trimethylbenzene in a CREC riser simulator. A heterogeneous model with adsorption and reaction phenomena.. *Ind & Eng Chem Res*. 2003;42:4162-4173.
37. Tonetto G, Ferreira ML, de Lasa HI. Steam promoted mesoporosity in USY zeolites: structural properties and 1,2,4-TMB reactivity. *J of Molecular Catalysis A: Chem*. 2004;216:83-99.
38. Gola A, Rebours B, Milazzo E, Lynch J, Benazzi F, Lacombe S, Delevoye L, Fernández C. Effect of leaching agent in the dealumination of stabilized Y zeolites. *Microporous and Mesoporous Materials*. 2000;40: 73-83.
39. Dudek MJ, Ponder JW. Accurate modeling of the intramolecular electrostatic energy of proteins. *J of Comp Chem*. 1995;16:791-816.
40. Horvath G, Kawazoe K. Method for the calculation of the effective pore size distribution in molecular sieve carbon. *J of Chem Eng of Jap*. 1983;16:470-475.
41. de la Puente G, Sedran U. Influence of dealumination on the micropore adsorption in FCC catalysts. *Microporous Materials*. 1997;12(4-6):251-260.
42. de la Puente G, Sedran U. Influence of dealumination on the micropore adsorption in FCC catalysts. *Microporous Materials*. 1997;12:251-260.
43. Fernández C, Vedrine J, Grosmangin J, Szabo G. Dealumination of an offretite-type zeolite: framework modifications. *Zeolites*. 1986;6:484-490.
44. Satterfield CN. *Heterogeneous Catalysis in Practice*. New York: McGraw Hill; 1980.
45 Kikuchi E, Matsuda T, Fujiki H, Morita Y. Disproportionation of 1,2,4-trimethylbenzene over montmorillonite pillared by aluminium oxide. *Appl Catalysis*. 1984, 11, 331-340.
46. Csicsery SM. Shape-selective catalyst. In: *Rabo JA. ACS Monograph: Zeolite Chemistry and Catalysis*. Washington: American Chemical Society. 1976;171:285-331. ACS Symposium Series, 171 (Zeolite chemistry and catalysis). Washington, DC: American Chemical Society, 1976:680-713.
47. Csicsery S. Selective disproportionation of alkylbenzenes over mordenite molecular sieve catalyst. *J of Catalysis*. 1970;19:394-397.
48. Csicsery S. The cause of shape selectivity of transalkylation in mordenite. *J of Catalysis*. 1971;23:124-130.
49. Ginsburg JM, Pekediz A, de Lasa HI. The CREC fluidized riser simulator. Characterization of mixing patterns. *Int J of Chem Reactor Eng*. 2003**;**1(A52):1-12.
50. Ko A, Kuo CT. Isomerization and disproportionation of 1,2,4-trimethylbenzene over HY zeolite. J of the Chinese Chem Soc. 1994;41:141-150.
51. Al-Khattaf S, de Lasa HI. Catalytic cracking of cumene in a riser simulator: a catalyst activity decay model. *Ind &.Eng Chem Res*. 2001;40: 5398-5404.
52. Coleman TF, Li Y. An interior, trust region approach for nonlinear minimization subject to bounds. *SIAM J on Optimization*. 1996;6:418-445.
53. Auerbach S, Jousse F, Vercauteren D. Dynamics of sorbed molecules in zeolites. In: Catlow CRA, van Santen, RA, Smit B. *Computer Modelling of Microporous and Mesoporous Materials*. Amsterdam: Elsevier; 2004: 49-108.
54. Al-Khattaf S, de Lasa HI. The role of diffusion in alkyl-benzenes catalytic cracking. *ApplCatalysis A*. 2002;226:139-153.
55. Chem3D-manual (http://www.camsoft.co.kr/support/documentation/manuals.htm)
56. Gnep N, Tejada J, Guisnet M. Mise au point d'une reaction simple de caractérisation du réseau poreux des zéolithes de taille de pore intermédiaire. Bulletin de la Société Chimique de France. 1982;1-2:5-11.
57. Satterfield CN, Cheng CS. Single-component diffusion of selected organic liquids in type Y zeolites. In: Baker GK, Lee MNY, Zwiebel I. *Adsorption Technology*. New York: AIChE Symposium Series, 1971,117, 67, 43-50.
58. Hasting SH, Nicholson DE. Thermodynamic equilibria among benzene and the methylbenzenes from spectroscopy data. *J of Chem and Eng Data*. 1961;6:1-4.
59. Brunauer S. *The Adsorption of Gases and Vapours*. Oxford: Oxford University Press; 1945.
60. Lippens B, De Boer J. Studies on pore systems in catalysts: V. The t method. *J of Catalysis*. 1965;4:319-323.
61. Cheng L, Yang R. Improved Horvath-Kawazoe equations including spherical pore models for calculating micropore size distribution. *Chem Eng Sci*. 1994;49:2599-2609.

Manuscript received Dec. 9, 2004, and revision received Jun. 1, 2005.